XL CILAMCE
IBERO-LATIN AMERICAN CONGRESS ON COMPUTATIONAL METHODS IN ENGINEERING
NOVEMBER 11-14, 2019
Praiamar Natal Hotel & Convention Natal, RN-BRAZIL

2D HYDROMECHANICAL MODELING OF WATERFLOODING IN FRACTURING CONDITIONS USING FINITE ELEMENTS WITH HIGH ASPECT RATIO

Matheus N. C. Brunet
Bruno M. C. M. Maciel
Igor F. Gomes
Leonardo J. N. Guimarães
matheus.brunet@ufpe.br
bruno.canabarro@ufpe.br
gomes@ufpe.br
leonardo@ufpe.br
Civil Engineering Department – Federal University of Pernambuco - UFPE
Av. da Arquitetura - Cidade Universitária, Recife - PE, 50740-540

Abstract. Waterflooding is a widely used methodology in the oil & gas industry and its main objective is to guarantee the pore pressure maintenance in reservoirs during production as well as to sweep the oil towards the producing wells. Injection of water in pressure conditions that exceed the reservoir fracture pressure in operations known as IAFP (Injection Above Fracture Pressure) it's often necessary to ensure the high injection rates required in secondary recovery processes. In order to model the hydromechanical behavior of the fracking in the presence of producing wells, which particularly occurs in IAFP operations, this work used the finite element method in two dimensions with high aspect ratio elements and a constitutive law based on the tensile damage mechanics to model the opening and propagation of hydraulic fractures. The fluid flow was described by Darcy's law and the fully coupled method was used to solve the hydromechanical equations. Numerical examples with different injection rates and production pressures were performed in order to verify the ability of the method to reproduce the opening and propagation of fractures in the presence of producing wells. The results showed the method was able to reproduce the opening and propagation of fractures in IAFP conditions and they also suggest that in some cases the producing wells can play an important role in the propagation length of the fractures.

Keywords: Hydraulic fractures, Finite elements with high aspect ratio, hydromechanical analysis

1 Introduction

Waterflooding is a secondary recovery method widely used in oil & gas industry to maintain reservoir pressure during oil production or to restore the pore pressure after depletion promoted by primary recovery. The injected water works like a piston by pushing the oil present in the reservoir towards producing wells. Craft and Hawkins [1].

The low quality of injected water is one of the causes for loss of injectivity around the injection wells and makes impossible reaching the design flows without an increasing in bottom hole pressure Gadde and Sharma [2].

A possible solution to the problem of pore plugging is the injection above fracture pressure (IAFP) even when the quality of injected water is very low. However, despite an important alternative, fracture behavior during injection must be predicted to avoid a reduction in reservoir performance due to anticipated water breakthrough and environmental problems due to a fracturing of adjacent layers Pedroso et al. [3]

It's well established the reservoir engineering parameters as the voidage replacement ratio and the well spacing and pattern may have a great relevance in fracture propagation. The voidage ratio can be defined as the relationship between injected water volume and produced fluids. Overproduction (Vr<1) stabilizes the dynamic fractures while overinjection (Vr>1) promotes an increase in fracture propagation van den Hoek et al. [4] and Eltvik et al. [5]

The studies proposed in this work aimed to model the hydromechanical behavior of the fracking in the presence of producing wells, which particularly occurs in IAFP operations, and analyze if the interface elements can represent fracture opening and propagation under IAFP conditions.

2 Methodology

This work used the finite element method in two dimensions. The mesh fragmentation technique presented in Manzoli, et al. [6], Sanchez, et al. [7] was used to insert the high aspect ratio elements and the constitutive law based on the tensile damage mechanics to model the opening and propagation of hydraulic fractures.

The high aspect elements were inserted between the regular FEM mesh through p3matpac package, the generator designed in MATLAB © software environment by Computational Geomechanics Method Group (LMCG).

In this paper the numerical analyses were performed by CODE_BRIGHT (COupled DEformation, BRIne, Gas and Heat Transport) Olivella, et al. [8], Oliver and Manzoli [9] and Guimarães, et al. [10]. The CODE_BRIGHT is a finite element procedure that performs numerical analysis of fluid flow in a deformable porous media in a fully coupled scheme.

2.1 Solid Finite Elements with High Aspect Ratio

Consider a solid finite element of three nodes with base b formed by the straight segment between nodes 2 and 3, and height h, being defined by the distance between node 1 and its projection in the base (1 '), in a system of axes coordinates (n, s), where n is normal to the base of the element, as shown in Figure 1. When $h \rightarrow 0$ this element presents a high aspect ratio of the largest to the smallest dimension (b/h) (Fig. 1).

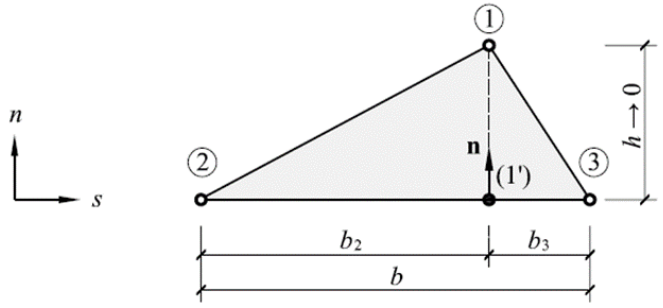

Figure 1. Three nodes solid finite element with high aspect ratio (adapted from Maedo [11]).

Mechanical behavior of the finite elements with high aspect ratio: The components of the approximation of the field of strain of the element given by Eq. (1) Gosz [12].

$$\{\epsilon\} = [\mathbf{B}]\{\mathbf{d}\} \Rightarrow \begin{Bmatrix} \epsilon_{nn} \\ \epsilon_{ss} \\ \gamma_{ns} \end{Bmatrix} = \begin{Bmatrix} \frac{u_n^{(1)} - \left(\frac{b_3}{b}\right)u_n^{(2)} - \left(\frac{b_2}{b}\right)u_n^{(3)}}{h} \\ \frac{(u_s^{(3)} + u_s^{(2)})}{b} \\ \frac{(u_n^{(3)} - u_n^{(2)})}{b} + \frac{u_s^{(1)} - \left(\frac{b_3}{b}\right)u_s^{(2)} - \left(\frac{b_2}{b}\right)u_s^{(3)}}{h} \end{Bmatrix}. \tag{1}$$

Where $\{\epsilon\}$ is the strain vector, $[\mathbf{B}]$ is the matrix of the derivatives of the form functions and $\{\mathbf{d}\}$ is the nodal displacement vector. $un^{(i)}$ and $us^{(i)}$ are components of the displacement of node i in a system of axes coordinates (n, s).

The deformation tensor $\{\epsilon\}$ can be decomposed into two parts, where $\tilde{\epsilon}$ contains the terms that depend on the base b and $\hat{\epsilon}$ contains the terms that depend on the height h, in general, for any system of coordinate axes (Eq. 2).

$$\epsilon = \tilde{\epsilon} + \frac{1}{h}(\boldsymbol{n} \otimes [\![\boldsymbol{u}]\!])^S. \tag{2}$$

When the height $h \rightarrow 0$, the component $\tilde{\epsilon}$, which is independent of h, remains limited, while the component $\hat{\epsilon}$ becomes unlimited and the deformations of the interface element are defined almost exclusively by the displacement of node (1) and its projection $(1')$ at the base of the element, it shows that the relative displacement vector $[\![\boldsymbol{u}]\!]$ corresponds to a discontinuous in the field of element displacements (strong discontinuous) Oliver and Manzoli [9], Maedo [11] and Cleto [13].

Hydraulic behavior of the finite elements with high aspect ratio: It is possible to extend the technique to represent the hydromechanical phenomena present in the hydraulic fracturing process. The gradient of the pressure field approximation in the given element is presented by Eq. (3) Cleto [13], Seixas [14], Maciel [15].

$$\nabla p_w = \begin{Bmatrix} \frac{1}{b}\left(p^{(3)} - p^{(2)}\right) \\ \frac{1}{h}[\![p]\!] \end{Bmatrix}. \tag{3}$$

Where ∇p_w is the pressure field gradient inside the element, $p^{(i)}$ corresponds to the pressures on the nodes 1, 2 and 3. $[\![p]\!] = p^{(1)} - p^{(1')}$ corresponds to the pressure jump and it corresponds to the difference of pressure between the node (1) and its projection on the base of the element $(1')$. We can decompose the flow in the element $\boldsymbol{q_w}$ into two parts, where $\tilde{\boldsymbol{q}}_{\boldsymbol{w}}$ contains the terms that depend on the base b and $\hat{\boldsymbol{q}}_{\boldsymbol{w}}$ contains the terms that depend on the height h (Eq. 4).

$$\boldsymbol{q_w} = \tilde{\boldsymbol{q}}_{\boldsymbol{w}} + \hat{\boldsymbol{q}}_{\boldsymbol{w}} = -\frac{(k/\mu_w)}{b}\begin{Bmatrix} p^{(3)} - p^{(2)} \\ 0 \end{Bmatrix} - \frac{(k/\mu_w)}{h}\begin{Bmatrix} 0 \\ [\![p]\!] \end{Bmatrix} \tag{4}$$

Note that when the height $h \rightarrow 0$, the flow of the element tends to infinity, which is physically impossible. In order that the flow in the element does not assume extremely high values and remains limited, when height $h \rightarrow 0$, the pressure difference between the node (1) and its projection at the base of the element (1 ') should tend to zero $[\![p]\!] \rightarrow 0$, it maintains the physical coherence appropriate to the problem. Note also that the first component of the flux in is proportional to the difference between the nodal pressure of the nodes 3 and 2, respectively. Therefore, the solid element acts as an one-dimensional element conducting the flux along the interface element.

Mesh Fragmentation Technique: The mesh fragmentation technique Manzoli, et al. [6] and Sanchez, et al. [7] consists of inserting interface elements (finite elements of high aspect ratio) between the regular elements of a finite element mesh, it allows to reproduce the effects of the process of formation, propagation and / or reactivation of fractures. The fracturing process occurs in the interface elements, which assigns a model of tensile damage, it enables them to have non-linear behavior. The elastic linear model is used in the regular elements.

The Figure 2 illustrates the steps of the 2D mesh fragmentation technique. First, the original coordinates of the nodes will be altered, reducing the size of the finite elements of the original mesh (regular elements) (Fig. 2a), creating a small space between adjacent elements (Fig. 2b) where it's inserted a pair of finite interface elements (finite elements of high aspect ratio) (Fig. 2c and Fig. 2d).

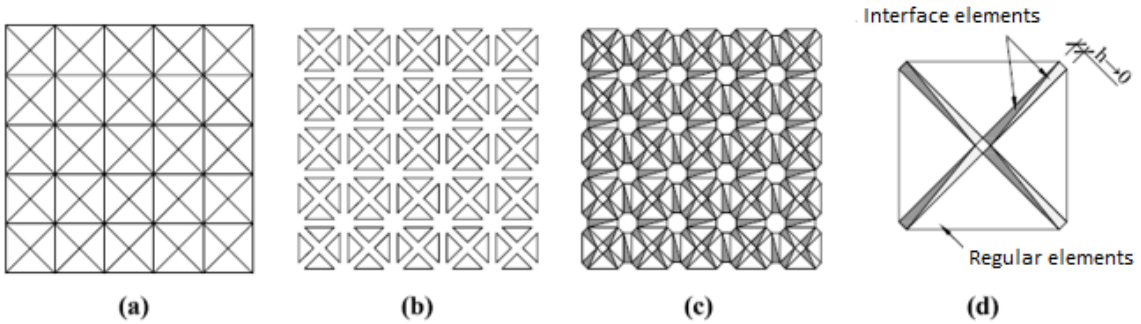

Figure 2. 2D mesh fragmentation technique. (a) original mesh; (b) fragmented mesh; (c) mesh with interface elements between the regular elements; (d) pair of interface elements between the regulator elements (adapted from Maedo [11]).

2.2 Tensile Damage Constitutive Model

In this work the model of tensile damage presented by Sánchez, et al. [7]. was adopted. The constitutive law for this model, instead of using scalar tensions, uses stress tensor (Eq. 5).

$$\boldsymbol{\sigma} = (1 - d)\overline{\boldsymbol{\sigma}}. \tag{5}$$

The variable $\boldsymbol{\sigma}$ is the apparent stress tensor, $d \in [0,1]$ is the damage and $\overline{\boldsymbol{\sigma}}$ is the elastic tensor of effective stresses. The damage criterion, which defines the elastic domain, is defined by Eq. (6).

$$\phi(\boldsymbol{\sigma}) = \tau(\boldsymbol{\sigma}) - q(r) \leq 0. \tag{6}$$

Where τ is the equivalent tensor that defines the elastic domain and q and r are the internal variables of the stress and strain, respectively. In the mesh fragmentation technique, the stress tensor $\boldsymbol{\sigma}$ is projected in the direction normal to the fracture surface (element base), resulting in the vector of stresses $\boldsymbol{T}$ and its normal component σ_n. In the model of tensile damage adopted, we use the law of exponential softening, which considers the fracture energy of the material and the thickness of the interface element, according to the Eq; (7).

$$q(r) = f_t e^{\frac{f_t^2}{G_f E} h(1 - r/f_t)} \tag{7}$$

Where f_t is the tensile strength, G_f is the fracture energy, E is the modulus of elasticity and h is the thickness of the interface element.

2.3 Permeability Evolution Law

The hydromechanical coupling of the hydraulic fracturing problem can be defined by the evolution of the fracture permeability as a function of the displacement jump calculated by the mechanical problem. The permeability variation in the interface element is given by the Eq. (8) Snow [16].

$$K = [\![u]\!]_n{}^2/12 \tag{8}$$

Where $[\![u]\!]_n$ is the jump component of the displacement field projected in the direction normal to the fracture. The jump component is calculated as a function of the volumetric deformation of the interface element and the thickness h.

3 Numerical Study of Fracturing Propagation

The studies proposed in this work aimed to analyze if the interface elements can represent fracture opening and propagation under IAFP conditions.

Geometry, Rock and Fluid Properties: Figure 3 and Table 1 present the geometry dimensions, the boundary conditions and the rock and fluid properties adopted across the entire media. In this work, the wells are nodes of the finite element mesh. The simulations were performed considering plane strain. Near the injection well (yellow region) it was adopted a low permeability media; its properties are shown in Table 1.

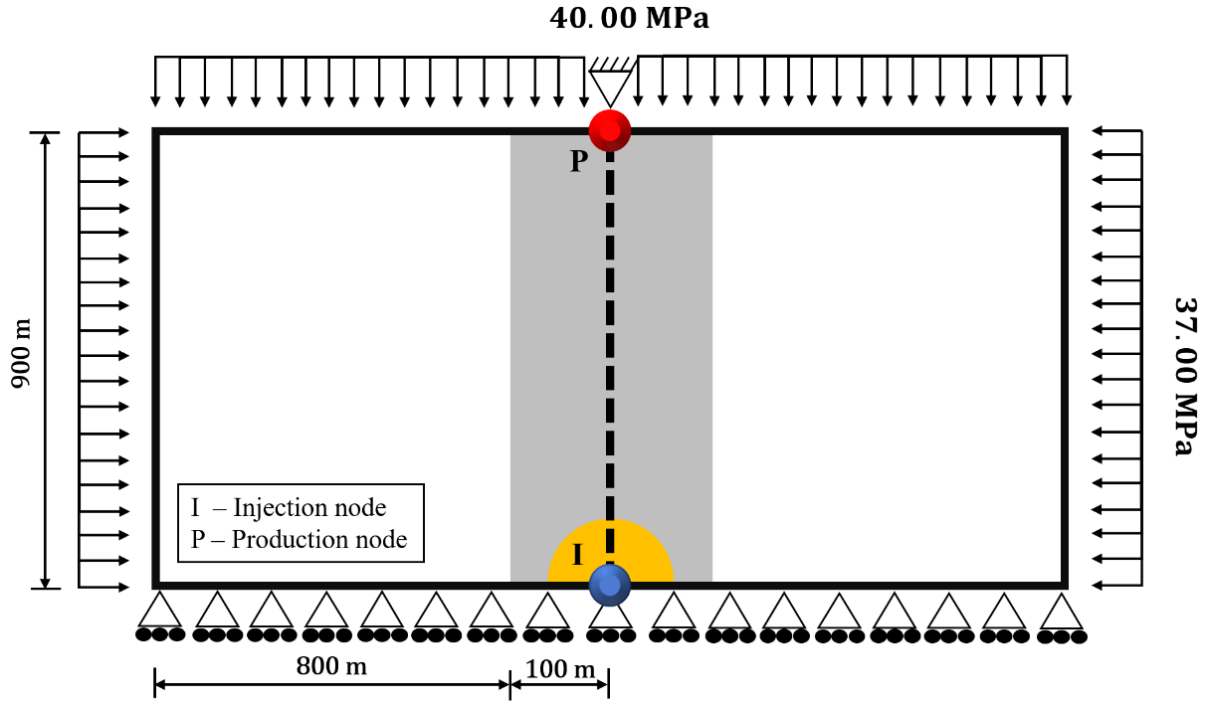

Figure 3: Region geometry and boundary conditions. (I) injection well and (P) production well.

Table 1. Rock and fluid properties

Properties	Nomenclature	Value
Young modulus (GPa)	E	20.00
Poisson's ratio	ν	0.25
Biot's coefficient	α	1.00
Tensile strength (MPa)	τ	1.50
Fracture energy (N/m)	G_f	140.00
Porosity	ϕ_m - ϕ_d	0.20 - 0.15
Permeability (m^2)	κ_m - κ_d	4.9×10^{-13} - 4.9×10^{-14}
Fluid density (Kg/m^3)	ρ	1000 (Kg/m^3)
Fluid viscosity (Pa.s)	μ	3.00×10^{-3}
Initial pore pressure (MPa)	P_0	30.00
Reservoir original height	Δz	50.00

*d – Damaged zone near injection well
*m – Matrix

The finite element mesh utilized in this work has 47452 triangular elements with a refinement of 1 m in the central region of geometry (gray region) and 200 m in the corners of the geometry (Figure 4). Only the central region was fragmented and the thickness of h=0.01m (1% of regular elements) was attributed to the interface elements.

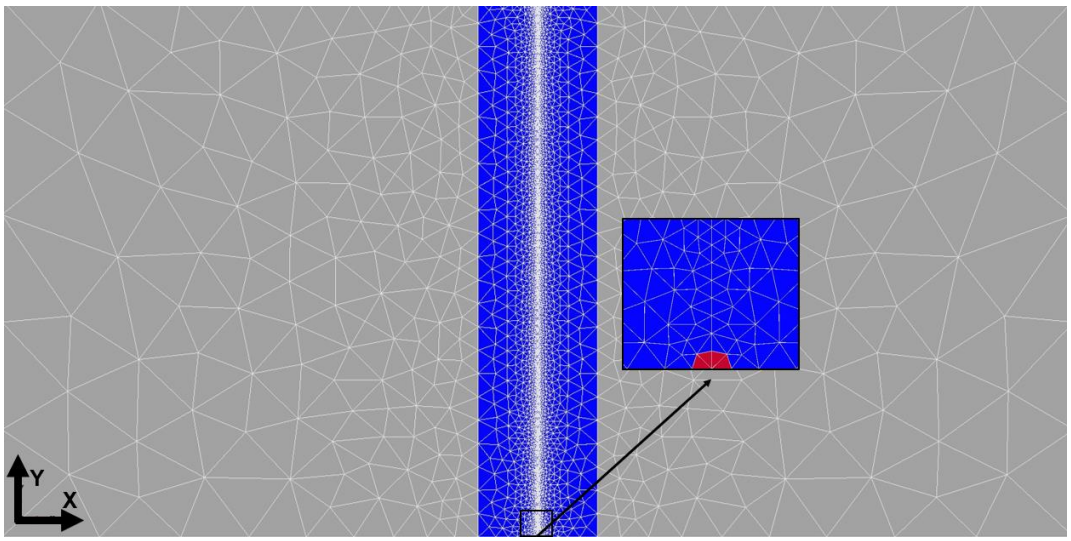

Figure 4: Geometry and finite triangular elements; Refined mesh near the fracture.

Breakdown pressure and fracture propagation pattern: The objective of these simulations was to obtain the breakdown pressure and the fracture propagation direction using interface elements. For that, a three-interval cycle of only injection was performed using a high viscosity fluid (9×10^{-3} Pa.s). In the first interval, the injection rate was increased linearly until reaching the final rate of 4.05×10^{-4} m^3/s. In the second interval the injection rate of 4.05×10^{-4} m^3/s was kept constant. In the third interval the injection was interrupted. The pressure versus time curve was recorded.

Injection rate effect on fracture propagation: In this study, a constant production pressure of 27 MPa and different injection rates were employed. Table 2 shows the flow rates of the injection well and the nomenclature for each case. The positions of the injection and production wells are (900,0) m and (900,900) m, respectively.

Table 2. Nomenclature of injection rate effect cases

Injection Rate	Nomenclature
6.94 x 10^{-4} (m^3/s)	C6000_27
6.36 x 10^{-4} (m^3/s)	C5500_27
5.78 x 10^{-4} (m^3/s)	C5000_27
5.78 x 10^{-4} (m^3/s)	C4000_27

Production pressure effect on fracture propagation: In this study, a constant injection rate of 6.94 x 10^{-4} m^3/s and different production pressures were employed. Table 3 shows the production pressures of the production well and the nomenclature for each case. The positions of the injection and production wells are (900,0) m and (900,900) m, respectively.

Table 3. Nomenclature of production pressure effect cases

Production pressure (MPa)	Nomenclature	Pressure drop
27.00	C6000_27	10.0%
26.25	C6000_26	12.5%
25.50	C6000_25	15.0%
24.00	C6000_24	20.0%

4 Results and Discussion

Breakdown pressure and fracture propagation pattern: Figure 5 shows the pressure versus time curve for the simulation involving only the injection of a viscous fluid.

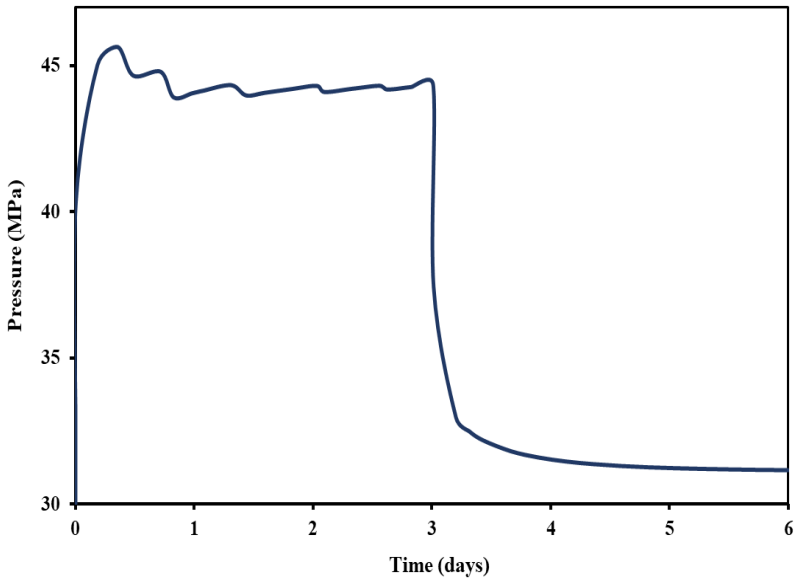

Figure 5: Pressure versus time for injection at three intervals using a viscous fluid.

Based on Figure 5, it was possible to obtain a simulated breakdown pressure (maximum injection pressure) of 45.6 MPa. This value is 7.3 % higher than the analytically calculated pressure. During the constant injection time, it was possible to see that the injection pressure was again above the analytically calculated propagation pressure and with a "saw-tooth" behavior. Throughout the shut-in time, the pressure decreases quickly approaching the reservoir pore pressure. For all simulations presented in this work, the hydraulic fractures propagated in the perpendicular direction to the Shmin. Pressure values slightly higher than the analytical values may be associated with the high leak-off of the porous media. According to Feng and Grey [17] formations with high permeability may present high values of breakdown and propagation pressure when compared to low permeability rocks. Because of

the high leak-off of permeable rocks, it is necessary to have a higher net fracture pressure for the opening and the propagation of fractures. The same explanation applies to saw-tooth behavior during fracture propagation. According to the authors, the fracture will propagate when the stored energy (pressure) reaches critical fracture energy for a portion of the rock. After that, the high leak-off values do not allow the pressure to reach the fracture propagation pressure for the next portion of rock and it makes necessary a pressure increase.

Injection rate effect on fracture propagation: Figure 6 shows the length of fractures for a constant production bottom hole pressure and different injection rates. The results showed that keeping a constant BHP the higher injection rates resulted in longer fracture lengths. The results additionally showed that the fractures reach a maximum length and then they remain with an approximately constant length.

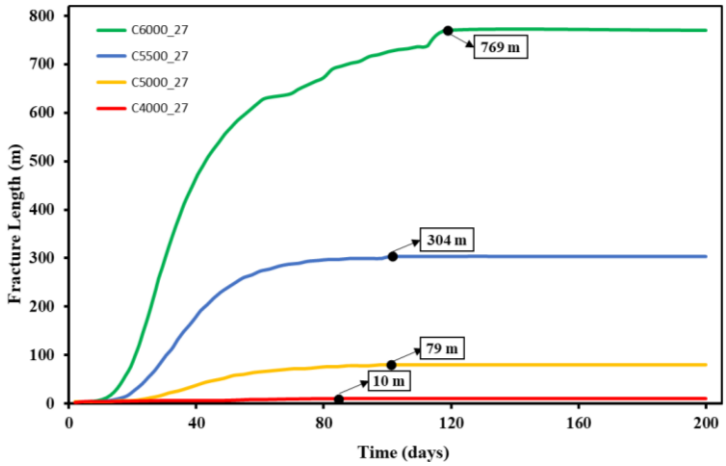

Figure 6: Fracture length (m) vs. time (days) for a constant production BHP and different injection rates.

According to van den Hoek [4] the length of fractures in the scheme of constant production BHP is strongly dependent on the transient flow regime and the average reservoir pressure. After the transient flow regime (steady-state regime) the voidage replacement ratio (Vr) is equal to 1 and there is no fracture propagation. Thus, the higher the injection rate imposed, the greater the pressure in the transient flow regime and the longer the hydraulic fracture length.

Production pressure effect on fracture propagation: The Figure 7 shows the length of fractures for a constant injection rates and different bottom hole pressure.

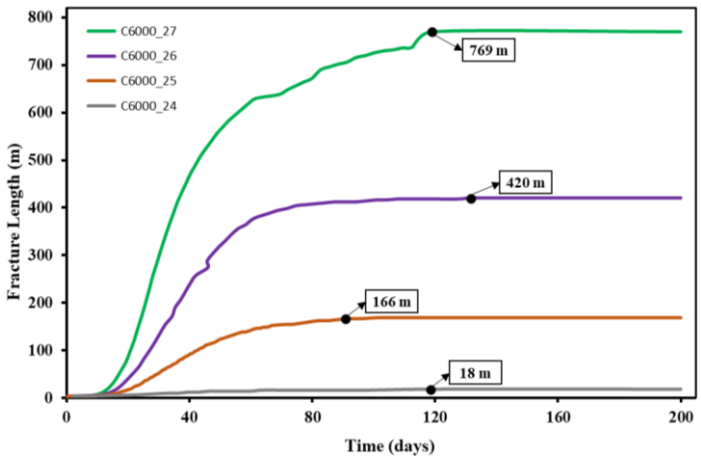

Figure 7: Fracture length (m) vs. time (days) for a constant injection rates and different production BHP.

Figure 7 shows that for higher production pressures when keeping the injection rate constant, the hydraulic fracture length increases. As discussed earlier, fracture length is strongly affected by average reservoir pressure. Consequently, for higher producer BHP the average reservoir pressure remains higher and the difference between fracture pressure and reservoir pressure remains smaller facilitating fracking.

5 Conclusions

The results showed that hydraulic fractures formed in waterflooding operations can reach hundreds of meters in length. It confirms the importance of this study for water injection operations more efficient and safer. The results also reinforce that fracture length is strongly affected by average reservoir pressure because the higher the average reservoir pressure the smaller is the difference between the average reservoir pressure and the fracture pressure. It was possible to confirm these results by changing injection rates and bottom hole production pressure. Finally, the results validate that the high aspect ratio finite element method using the constitutive model of tensile damage can capture the central aspects of hydraulic fracturing in the presence of production wells, which typically occurs in injection above fracture pressure operations.

Acknowledgements

The authors are grateful to Federal University of Pernambuco, National Council for Scientific and Technological Development (CNPq), Computational Geomechanics Method Group (LMCG), Energi Simulation and Petrobras for the support of this work.

References

[1] B. C. Craft, M. Hawkins. Applied Petroleum Reservoir Engineering. Revised by R. E. Terry, J. B. Rogers. Pearson Education, 2015.

[2] P. B. Gadde and M. M. Sharma, 2001. Growing injection well fractures and their impact on waterflood performance. *SPE Annual Technical Conference and Exhibition. Society of Petroleum Engineers.*

[3] C. A. Pedroso, L. C. C. Marques, P. R. M. Pires, L. C. A. Paixao, E. B. L. Junior, 2009. Analysis of Fracture Growth Induced by the Injection of Water Above the Fracture Pressure in Nonconsolidated Sandstones and Soft Carbonates - Deviations from the Linear Elastic Elastic Model or Why Can't I Inject Even Above the Fracture Pressure?. *SPE European Formation Damage Conference.*

[4] P.J. van den Hoek, B. Hustedt, M. Sobera, H. Mahani, J. Snippe and D. Zwarts, 2008. Dynamic Induced Fractures in Waterfloods and EOR. *SPE Russian Oil & Gas Technical Conference and Exhibition.*

[5] P. Eltvik,T. Skoglunn, A. Settari, 1992. Waterflood-Induced Fracturing: Water Injection Above Parting Pressure at Valhall. *67th Annual Technical Conference and Exhibition of Society of Petroleum Engineers.*

[6] O. L. Manzoli et al, 2012. Modeling of interfaces in two-dimensional problems using solid finite elements with high aspect ratio. *Computers & Structures.* Vol. 94: 70-82.

[7] M. Sanchez, O. L. Manzoli, and L. N. Guimarães, 2014. Modeling 3-D desiccation soil crack networks using a mesh fragmentation technique. *Computers and Geotechnics*. Vol. 62: 27-39.

[8] S. Olivella et al. 1994. Nonisothermal multiphase flow of brine and gas through saline media. *Transport in Porous Media*. Vol. 15.

[9] J. Oliver, M. Cervera, O. Manzoli, 1999. Strong discontinuities and continuum plasticity models: the strong discontinuity approach. *International journal of plasticity.* Vol. 3: 319-351.

[10] L. J. N. Guimarães, A. Gens and S. Olivella, 2007. Coupled thermo-hydro-mechanical and chemical analysis of expansive clay subjected to heating and hydration. *Transport in Porous Media.* Vol. 66

[11] M. A. Maedo 2015. *Simulação computacional por elementos finitos de múltiplas fissuras em sólidos usando tecnica de fragmentação de malha*. City: Bauru, São Paulo State University.
[12] Gosz M. R. 2005. *Finite Element Method: Applications in Solids, Structures, and Heat Transfer (Mechanical Engineering).*
[13] P. R. Cleto, 2016. *Simulação de fraturamento hidráulico usando elementos finitos de elevada razão de aspecto com acoplamento hidromecânico.* City: Bauru, São Paulo State University.
[14] M. G. Seixas, 2015. *Modelagem hidromecânica do fraturamento hidráulico de rochas via elementos finitos com elementos especiais de interface.* City: Recife, Federal University of Pernambuco
[15] B. M. C. M. Maciel, 2016. *Aplicação da técnica de fragmentação de malha com elementos finitos de alta razão de aspect para a simulação de fraturamento hidráulico.* City: Recife, Federal University of Pernambuco
[16] D. T. Snow, 1965. A parallel model of fractured permeable media. PhD thesis, University of California.